

**X-ray Monitoring of the Magnetar CXOU J171405.7–381031 in SNR CTB 37B**E. V. GOTTHELF,<sup>\*</sup> J. P. HALPERN,<sup>†</sup> K. MORI,<sup>†</sup> AND A. M. BELOBORODOV<sup>†</sup>

## ABSTRACT

We present the results of our 8 year X-ray monitoring campaign on CXOU J171405.7–381031, the magnetar associated with the faint supernova remnant (SNR) CTB 37B. It is among the youngest by inferred spin-down age, and most energetic in spin-down power of magnetars, and may contribute, at least partially, to the GeV and TeV emission coincident with the SNR. We use a series of *Chandra*, *XMM-Newton*, and *NuSTAR* observations to characterize the timing and spectral properties of the magnetar. The spin-down rate of the pulsar almost doubled in  $< 1$  year and then decreased slowly to a more stable value. Its X-ray flux varied by  $\approx 50\%$ , possibly correlated with the spin-down rate. The 1 – 79 keV spectrum is well-characterized by an absorbed blackbody plus power-law model with an average temperature of  $kT = 0.62 \pm 0.04$  keV and photon index  $\Gamma = 0.92 \pm 0.16$ , or by a Comptonized blackbody with  $kT = 0.55 \pm 0.04$  keV and an additional hard power law with  $\Gamma = 0.70 \pm 0.20$ . In contrast with most magnetars, the pulsed signal is found to decrease with energy up to 6 keV, which is apparently caused by mixing with the hard spectral component that is pulse-phase shifted by  $\approx 0.43$  cycles from the soft X-rays. We also analyze the spectrum of the nearby, diffuse nonthermal source XMMU J171410.8–381442, whose relation to the SNR is uncertain.

**Keywords:** ISM: individual (CTB 37B) — pulsars: individual (CXOU J171405.7–381031) — stars: neutron

## 1. INTRODUCTION

Modeling the spectra of magnetars provide an important diagnostic for understanding their emission mechanisms. Early literature characterized magnetars as “soft” X-ray sources emitting in the  $< 10$  keV X-ray band. Their spectra were typically fitted with blackbody emission from a hot spot(s) on the neutron star (NS) surface, plus a steep power-law component with photon index  $\Gamma \sim 4$ , possibly scattered from the magnetosphere (e.g., [Mereghetti & Stella 1995](#); [van Paradijs et al. 1995](#)). More recent *INTEGRAL* observations of the anomalous X-ray pulsar (AXP) subclass of magnetars revealed a previously unrecognized, flatter spectral component above  $\sim 10$  keV, extending up to  $> 100$  keV, with a pulse modulation that increases with energy. These hard X-rays, beginning

with detections of 1E 1841–045 ([Molkov et al. 2004](#)) 1RXS J170849.0–400910 ([Revnivtsev et al. 2004](#)), and 4U 0142+61 ([den Hartog et al. 2004](#)), are fitted with photon indices in the range  $\Gamma = 0.8 - 1.4$ , much harder than an extrapolation of the measured spectra below  $< 10$  keV. The majority of the luminosity of these objects is emitted above 10 keV in this hard spectral component.

Hard X-rays from magnetars must be produced by nonthermal particles in the magnetosphere. A mechanism for this emission was recently described by [Beloborodov \(2013a,b\)](#): electron-positron discharge creates relativistic particles with Lorentz factors  $\gamma \sim 10^3$  near the neutron star, the particles flow out along the extended magnetic field lines and decelerate with  $\gamma \propto B$ , losing energy to resonant scattering of thermal X-rays. The spectrum emitted by the decelerating plasma peaks above 100 keV, and its shape depends on the angle of the rotation axis to the line of sight. The model successfully reproduced the phase-resolved spectra of the aforementioned magnetars, the three best-studied objects ([Hascoët et al. 2014](#)). *NuSTAR* is well suited to studying the hard X-ray spectral components of magnetars, up to 79 keV. Its targets have included SGR J1745–2900 ([Mori et al. 2013](#); [Kaspi et al. 2014](#)),

Corresponding author: E. V. Gotthelf; [eric@astro.columbia.edu](mailto:eric@astro.columbia.edu)

<sup>\*</sup> Columbia Astrophysics Laboratory, Columbia University, 550 West 120th Street, New York, NY 10027-6601, USA.  
Departament de Física Quàntica i Astrofísica, Institut de Ciències del Cosmos, Universitat de Barcelona, IEEC-UB, Martí i Franquès 1, 08028, Barcelona, Spain.

<sup>†</sup> Columbia Astrophysics Laboratory, Columbia University, 550 West 120th Street, New York, NY 10027-6601, USA.

**Table 1.** Log of X-ray Observations of CXOU J171405.7–381031 in CTB 37B

Instrument/Mode <sup>a</sup>	ObsID	Date (UT) <sup>b</sup>	Exposure (ks) <sup>c</sup>	Epoch (MJD) <sup>d</sup>	Period (s)
<i>ASCA</i> GIS	54002030	1996 Sep 12	13.3	50338.9	3.7954(1)
<i>Suzaku</i> XIS	501007010	2007 Aug 27	82.8	53974.1	...
<i>Chandra</i> ACIS-I/TE/VF	6692	2007 Feb 2	25.2	54133.5	...
<i>Chandra</i> ACIS-S3/CC/F	10113	2009 Jan 25	30.1	54856.3	3.823056(17)
<i>Chandra</i> ACIS-S3/CC/F	11233	2010 Jan 30	30.1	55226.5	3.824936(18)
<i>XMM-Newton</i> EPIC pn/FF	0606020101	2010 Mar 17	93.0	55273.2	3.825353(4)
<i>XMM-Newton</i> EPIC pn/FF	0670330101	2012 Mar 13	11.5	55999.5	3.83039(4)
<i>Chandra</i> ACIS-S3/CC/F	13749	2012 Jul 16	20.1	56124.3	3.831062(29)
<i>Chandra</i> ACIS-S3/CC/F	16762	2015 May 4	20.1	57146.6	3.835459(31)
<i>NuSTAR</i> FPM	30001130002	2015 May 8	80.9	57151.1	3.8354346(69)
<i>Chandra</i> ACIS-S3/CC/F	16763	2015 Oct 13	19.2	57308.4	3.836025(38)
<i>NuSTAR</i> FPM	30201031002	2016 Sep 22	78.6	57654.9	3.8375205(57)
<i>XMM-Newton</i> EPIC pn/FF	0790870201	2016 Sep 23	27.5	57654.9	3.837494(18)
<i>XMM-Newton</i> EPIC pn/FF	0790870301	2017 Feb 22	20.0	57806.5	3.837980(20)

<sup>a</sup>Mission modes: *Chandra* Timed Exposure (TE), Continuous Clocking (CC), Faint Grading (F), Very Faint Grading (VF); *XMM-Newton* Full Frame (FF).

<sup>b</sup>Start date of observation.

<sup>c</sup>Effective exposure time for the EPIC pn after time filtering.

<sup>d</sup>Epoch of period is the mid-time of the observation.

1E 1841–045 (An et al. 2013, 2015), 1E 2259+586 (Vogel et al. 2014), 1E 1048.1–5937 (An et al. 2014; Yang et al. 2016), 4U 0142+61 (Tendulkar et al. 2015), SGR 1806–20 (Younes et al. 2017a), SGR J1935+2154 (Younes et al. 2017b), PSR J1622–4950 (Camilo et al. 2018), XTE J1810–197 (Gotthelf et al. 2019), and SGR 1900+14 (Tamba et al. 2019).

Aharonian et al. (2008) discovered the *Chandra* point source CXOU J171405.7–381031 in the supernova remnant (SNR) CTB 37B in a follow up effort to identify HESS J1713–381, a coincident TeV source (Aharonian et al. 2006). They considered the *Chandra* source a candidate pulsar, albeit with an unusually soft, non-thermal spectrum. Nakamura et al. (2009) analyzed *Chandra* and *Suzaku* spectra of CXOU J171405.7–381031 (hereafter J171405), suggesting that it is an AXP based on evidence of flux variability. Halpern & Gotthelf (2010a, Paper I) discovered 3.82 s pulsations from J171405 that verifies this conjecture. Halpern & Gotthelf (2010b, Paper II) and Sato et al. (2010) reported follow-up observations using *Chandra* and *XMM-Newton*, respectively, that measure the period derivative of the pulsar, establishing its quantitative magnetar properties. J171405 has a higher spin-down power and younger characteristic age than most

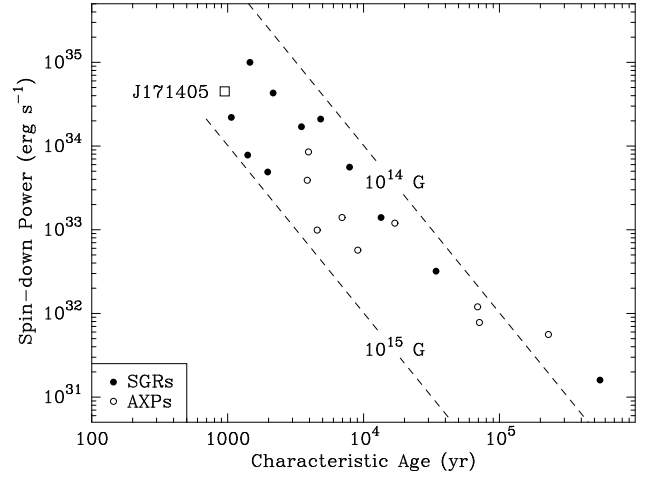


**Figure 1.** A summary of derived dipole spin-down properties of 21 magnetars based on period and period-derivative data during relatively quiescent periods, if available. Two magnetars with very small or unmeasured spin-down rates are omitted here.

magnetars (Figure 1), falling among the most energetic soft gamma-ray repeaters (SGRs). Its spin-down power is comparable to its X-ray luminosity.

Although HESS J1713–381 coincides with the SNR, its TeV structure has not been spatially resolved, and the young age and rapid spin-down of J171405 suggest

the possibility (Paper II) that the pulsar contributes to the TeV emission via inverse Compton scattering by a relic pulsar wind nebula (PWN). Moreover, the presence of the nearby unidentified hard, diffuse X-ray source XMMU J171410.8–381442 adds further uncertainty about the origin of the TeV emission.

As described in Section 2 we have obtained new *Chandra*, *XMM-Newton*, and *NuSTAR* observations of J171405 in order to monitor its timing and spectrum. A prime motivation was to search for any precursor of an impending SGR outburst, as may be anticipated from its location among the SGRs in Figure 1. A log of X-ray observations is presented in Table 1. In Sections 3–5 we describe the analysis of these data sets, along with available archival data spanning two decades. We show that the pulsar spins down erratically, and find that the *NuSTAR* X-ray observations clearly detect emission above 10 keV. In Section 5 we also provide a spectral analysis of the nearby hard, diffuse nonthermal source. Finally, we discuss our results in Section 6.

## 2. X-RAY OBSERVATIONS

### 2.1. *NuSTAR*

We observed J171405 twice with *NuSTAR*, on 2015 May 8 and 2016 September 22. *NuSTAR* consists of two co-aligned X-ray telescopes, with corresponding focal plane modules FPMA and FPMB that provide 18'' FWHM (1' HPD) imaging resolution over a 3–79 keV X-ray band, with a characteristic spectral resolution of 400 eV FWHM at 10 keV (Harrison et al. 2013). The reconstructed *NuSTAR* coordinates are accurate to 7''5 at the 90% confidence level. The nominal timing accuracy of *NuSTAR* is  $\sim 2$  ms rms, after correcting for drift of the on-board clock, with the absolute timescale shown to be better than 3 ms (Mori et al. 2014; Madsen et al. 2015).

*NuSTAR* data were processed and analyzed using FTTOOLS 09May2016\_V6.19 (NUSTARDAS 14Apr16\_V1.6.0) with *NuSTAR* Calibration Database (CALDB) files of 2016 July 6. The resulting data set provides a total of 80.9 ks and 78.6 ks of net good exposure time for the 2015 and 2016 pointings, respectively. For all subsequent analysis we merged data from both FPM detectors.

### 2.2. *Chandra*

Our previous *Chandra* observations of J171405 were reported in Papers I & II (see Table 1). We acquired three additional *Chandra* monitoring observations on 2012 July 16, 2015 May 4 (coordinated with our first *NuSTAR* observation), and 2015 October 13. The pulsar was located on the ACIS-S3 CCD and recorded in

continuous-clocking (CC) mode. This provided a time resolution of 2.85 ms and no spectral pile-up. This is the same instrumental setup as used previously and fully described in the earlier papers along with a description of their reduction and analysis. The photon arrival times are adjusted in the standard processing to account for the known position of the pulsar, spacecraft dither, and any SIM offset. All observations were free of enhanced background episodes and required no time filtering. Reduction and analysis used the standard software packages CIAO (v4.8) and CALDB (v4.1.1).

### 2.3. *XMM-Newton*

J171405 was observed four times using *XMM-Newton*, initially by Sato et al. (2001) and later as part of our monitoring program (see Table 1). In particular, our 2016 September 23 *XMM-Newton* observation was obtained simultaneously with *NuSTAR*. In this work, we concentrate on data from the three EPIC sensors on-board *XMM-Newton*, the pn detector (Strüder et al. 2001) and MOS1 and MOS2 (Turner et al. 2001). The pn consist of 12 segments and the MOS comprises a mosaic of seven CCDs. These detectors lie at the focal plane of coaligned replicated foil mirrors with a maximum effective area of  $A^{\text{eff}}(\text{pn}) \approx 1400 \text{ cm}^2$  and  $A^{\text{eff}}(\text{MOS1} + \text{MOS2}) \approx 1000 \text{ cm}^2$  at 1.5 keV. The FWHM of the on-axis point spread function (PSF) at 1.5 keV is  $\approx 12''.5$  and  $\approx 4''.3$ , for the pn and MOS, respectively. The EPIC detectors have a  $\approx 29'$  diameter field-of-view (FoV) and are sensitive to X-rays in the 0.15–12 keV range with moderate energy resolution of  $E/\Delta E(\text{pn}) \sim 20\text{--}50$ .

The *XMM-Newton* observations of J171405 were acquired with the EPIC pn operated in `FullFrameMode` with a sampling time of 73.4 ms. With the exception of the first observation, data collected by the two EPIC MOS detectors used the `SmallWindowMode` for which only a small portion ( $1'.8 \times 1'.8$ ) of the central CCD is read out in order to increase its time resolution to 0.3 s. The first observation (ObsID 0606020101) used `FullFrameMode` mode that allowed MOS imaging of the whole FoV at the nominal 2.6 s time resolution. (The MOS observations are not listed separately in Table 1.)

Data were reduced and analyzed using the Standard Analysis Software (SAS) v.15 with the most up-to-date calibration files. After filtering out background flares we obtained usable pn/MOS exposure time for the observations, ordered by time, of 93/93 ks, 11.5/16.6 ks, 27.5/29.1 ks, and 20.0/21.6 ks.

## 3. IMAGE ANALYSIS

The *XMM-Newton* data is most useful for mapping the supernova remnant flux from CTB 37B. This soft

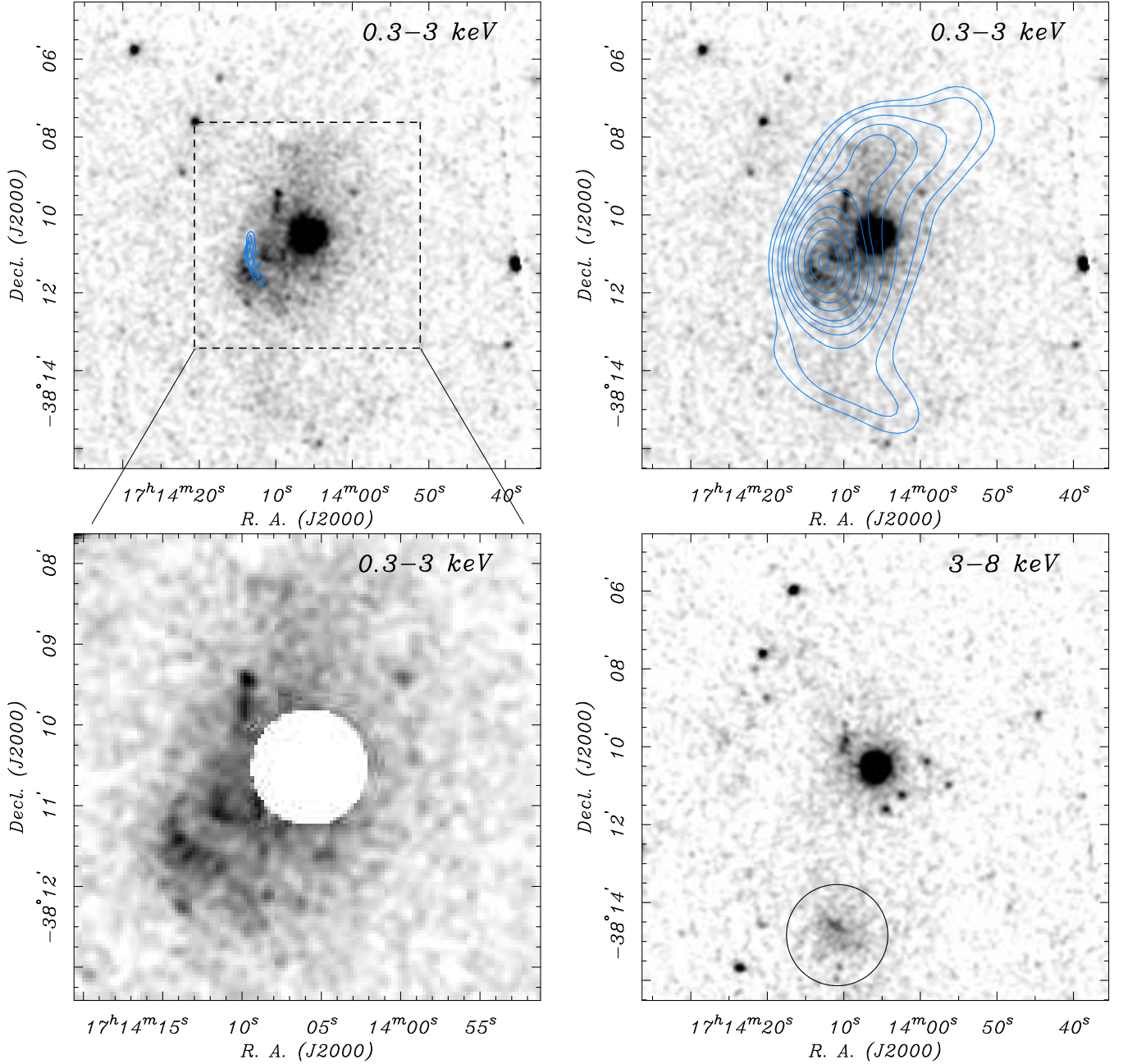


**Figure 2.** Exposure corrected, smoothed *XMM-Newton* EPIC MOS images of J171405 in CTB 37B, in two energy bands: 0.3–3 keV and 3–8 keV. These images are scaled logarithmically and stretched to highlight the diffuse emission. Diffuse thermal emission from the supernova remnant is clearly evident in the 0.3–3 keV band, overlapping the radio remnant (contours). The upper-left image shows the 20 cm contours from the Multi-Array Galactic Plane Imaging Survey (White et al. 2005), while the upper-right image shows the 843 MHz contours from the Molonglo Observatory Synthesis Telescope (Green et al. 1999). Details of X-ray structure of the remnant are shown with expanded scale in the lower-left image, with the magnetar region excluded. In the 3–8 keV band (lower right), the circle to the south south-east of the pulsar is the extraction aperture for the extended, hard source XMMU J171410.8–381442 analyzed in Section 5.2.



thermal X-ray emissions falls outside the *NuSTAR* energy band and the *Chandra* data contains only 1D spatial information. Figure 2 displays EPIC MOS images in two energy bands, above and below 3 keV. These exposure-corrected, smoothed images, combining data from all four *XMM-Newton* data sets, are scaled logarithmically and stretched to highlight the diffuse SNR emission prominent in the lower energy band. The bulk of the thermal emission lies in a region roughly  $3' \times 6'$  in extent and orientated with a P.A. of  $\sim 235^\circ$ . To the east, the emission is evidently delineated in part by the radio SNR shell fragment. On a larger scale there is weak evidence for very low surface-brightness, asymmetric X-ray emission, possibly up to  $\sim 7'$  from the magnetar, suggesting the true size of the SNR. Barely resolved, to the southeast, is a patch of radial striations extending between  $1'.7 - 2'.1$  that is not associated with any known PSF pattern. The structure in this feature is not resolved in the lower resolution EPIC pn images (not shown). Deep *Chandra* imaging-spectroscopy is required to further resolve and identify the nature of these striations.

In the higher energy band, above 3 keV, the field is dominated by the central magnetar with no clear evidence of SNR emission. Instead we find a distinct diffuse hard X-ray feature  $\approx 2'$  in diameter, first reported by Nakamura et al. (2009). This source is located  $4'.4$  south south-east of the magnetar with approximate coordinates (J2000.0) R.A. =  $17^h 14^m 10^s.8$ , decl. =  $-38^\circ 14' 42''$  (herein XMMU J171410.8–381442), and is not seen below  $< 3$  keV. It is not clear whether this hard source is associated with CTB 37B. We will explore its possible nature in Section 5.2.

#### 4. TIMING ANALYSIS

The erratic spin-down rates of magnetars is well documented, and a similar behavior has already been established for J171405 (see Paper II). Here we (re-)analyze all 8 years of accumulated timing observations of this magnetar to characterize its long-term spin-down evolution. For the following analysis, all photon arrival times are converted to barycentric dynamical time (TDB) using the DE405 solar system ephemeris and the *Chandra* position (J2000.0) R.A. =  $17^h 14^m 05^s.74$ , decl. =  $-38^\circ 10' 30''.9$  (Paper II). The timing methods used herein are generally described in Paper I.

Source lightcurves were generated for the *XMM-Newton* data using a  $30''$  radius aperture in the energy range 1–5 keV, optimal for maximizing the pulse signal. As the *Chandra* data was obtained in CC-mode, we extracted counts from the central four source columns ( $2''$  diameter), with the 1–5 keV energy cut. For *NuSTAR*,

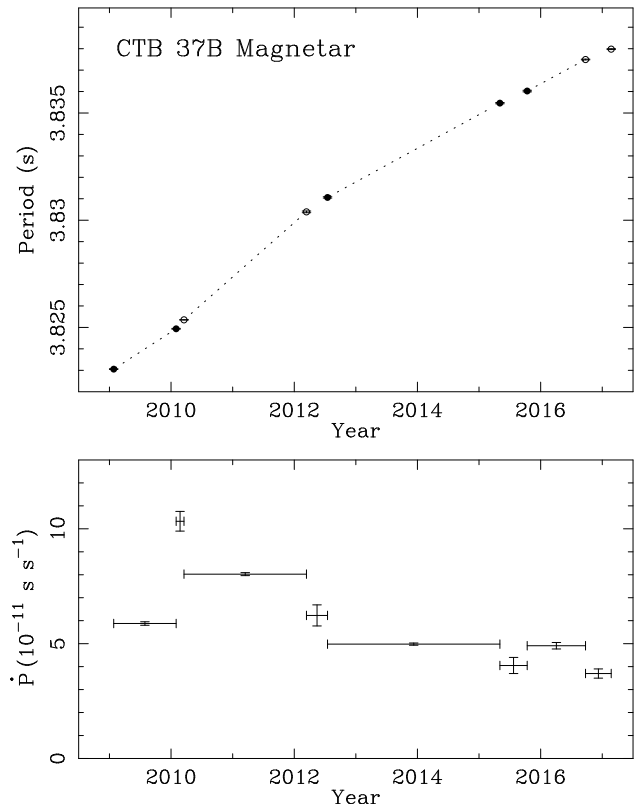


**Figure 3.** Top: Period measurements of J171405 from the five *Chandra* CC-mode observations (filled circles) and the four *XMM-Newton* observations. Error bars are smaller than the size of the symbols. Bottom: Period derivatives between consecutive measurements. The redundant *NuSTAR* points are not shown.

we extracted counts from a  $51''$  radius source aperture, including photons below the standard 3 keV spectral analysis threshold.

To determine the spin period of J171405 at each epoch, we searched around the nominal value using the  $Z_1^2$  test (Bucccheri et al. 1983), appropriate for the essentially sinusoidal pulse profile. The quoted 68.3% ( $1\sigma$ ) uncertainty in the period measurements are computed from the  $\Delta Z_1^2 (= \Delta \chi^2) = 1$  decrement resolved around the signal peak in the periodogram. The resulting period values are reported in Table 1 and are plotted in Figure 3, along with period derivatives, determined by subtracting periods between each epoch.

In early 2010 the period derivative quickly doubled, but it gradually returned to a more stable value of  $\dot{P} \approx 5 \times 10^{-11}$ . Because of the sparse and irregular monitoring, it is not possible to determine if additional, short episodes of enhanced spin-down occurred. There is one more pulsed detection, from archival *ASCA* data in 1996, which gives  $\dot{P} = 7.0 \times 10^{-11}$  between 1996 and 2010 (Paper II), possibly representative of a long-term,

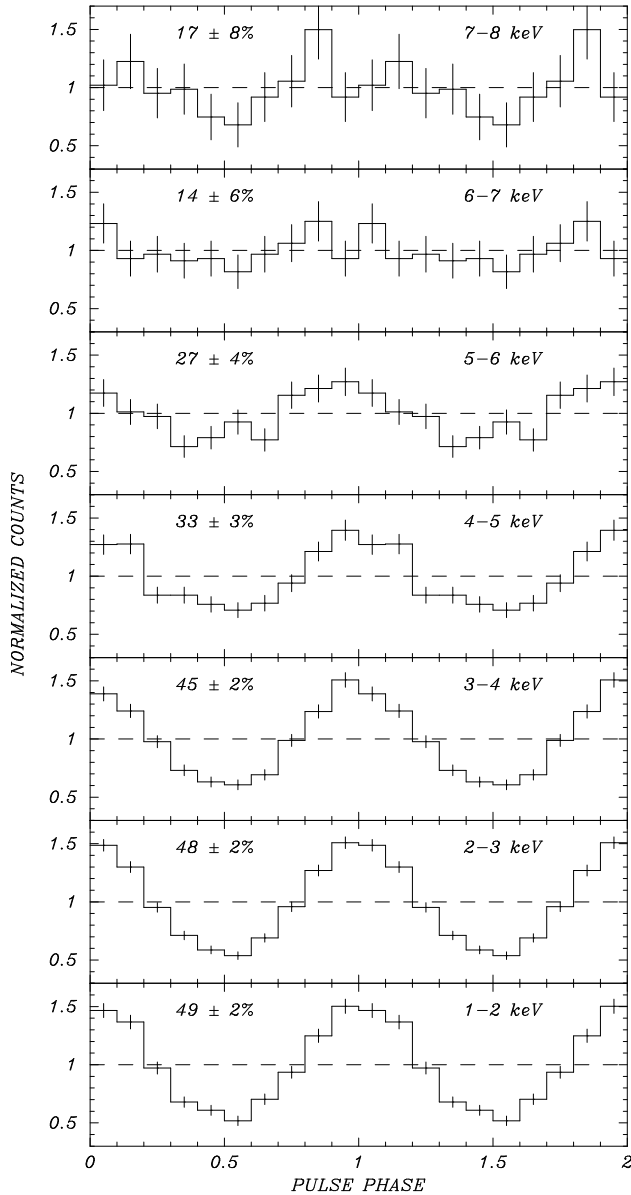


**Figure 4.** Pulse modulation of J171405 as a function of energy from the long, 2010 *XMM-Newton* observation. These profiles are background subtracted and normalized so that the pulsed fraction can be read from the y-axis. The pulsed signal decreases gradually with energy, approaching Gaussian fluctuations at 6–8 keV. This is further illustrated in Figure 7 for *NuSTAR* data.

average value. For clarity, we exclude the *ASCA* point in Figure 3.

The pulse profile appears to be generally stable in time and is well-modeled by a sinusoidal function  $y(\phi) = A \sin \psi + B$  with pulsed fraction  $f_p = A/B$ . For the four *XMM-Newton* epochs, the average background-subtracted pulsed fraction is  $\approx 44 \pm 4\%$  in the 1–5 keV band. As shown in Figure 4, we also examine the pulsed fraction as a function of energy using the deep 2010

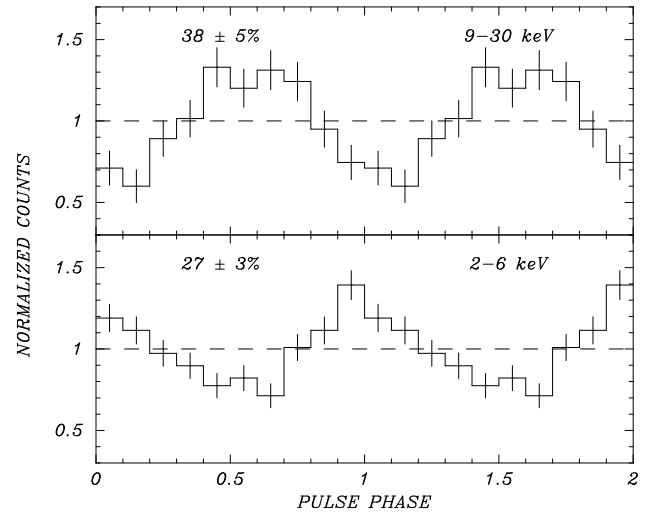


**Figure 5.** *NuSTAR* pulse profiles of J171405 computed in two energy bands, 2–6 keV and 9–30 keV, from the 2016 observation. These profiles are background subtracted and normalized so that the pulsed fraction is read from the y-axis. The  $180^\circ$  shift in phase from the soft to the hard band is additional evidence for a hard spectral component that dominates above 9 keV (see discussion in Section 5.1).

*XMM-Newton* observation. These data provide sufficient statistics to resolve a strong energy dependence in the modulation, which decreases with energy until reaching the  $3\sigma$  limit of 18% at  $\approx 6$  keV. This result is marginally reproduced in the other, much shorter *XMM-Newton* observations, but with less significance.

In the *NuSTAR* observations we at first found no evidence for a pulsed signal in the full spectral band. Below 6 keV, however, we recover the expected signal, consistent with the *XMM-Newton* results. Examining the modulation as a function of energy reveals a sinusoidal signal above 9 keV that is steadily increasing with energy, but phase shifted by  $\approx 180^\circ$  relative to the softer X-ray pulse profile. This is illustrated in Figure 5, showing the pulse profiles in the two energy bands of interest. This strongly suggests the presence of an independent hard spectral component dominating above 10 keV, consistent with that found for other magnetars, where the pulsed fraction increases with energy. However, the present *NuSTAR* data are insensitive to pulsations above 30 keV, where the signal is most likely masked by a relatively large background.

Given the strong energy dependence of the pulsed fraction, we postulate a model for the modulation that incorporates the overlapping, pulsed spectral components, including their phase difference. The hard and soft components combine to cancel out the modulation in their region of overlap. We also model the modulation in

**Table 2.** CXOU J171405.7–381031: Joint Fits to Coincident 2016 *XMM-Newton*/*NuSTAR* Spectra

Parameter	CBB+PL	CBB+PL	BB+PL	PL+PL
	Tuned			
$N_{\text{H}}$ ( $10^{22}$ cm $^{-2}$ )	$4.0 \pm 0.5$	$3.9 \pm 0.6$	$3.6 \pm 0.5$	$7.0 \pm 0.7$
$kT_1$ (keV)	$0.54 \pm 0.05$	$0.55 \pm 0.04$	$0.62 \pm 0.04$	...
$R_1$ (km)	$1.3(1.1 - 1.6)$	$1.3(1.1 - 1.4)$	$1.1(0.95 - 1.3)$	...
$L_{\text{bol}}^a$	...	...	$2.33 \times 10^{34}$	...
$\Gamma_1$	...	...	...	$3.94 \pm 0.4$
$\Gamma_2$	$0.59 \pm 0.22$	$0.70 \pm 0.20$	$0.92 \pm 0.26$	$0.48 \pm 0.2$
$\alpha$	$1.6(1.2 - 2.6)$	$2.1(\text{fixed}^b)$	...	...
$F_x(2 - 10 \text{ keV})^c$	$1.18 \times 10^{-12}$	$1.18 \times 10^{-12}$	$1.19 \times 10^{-12}$	$1.15 \times 10^{-12}$
$L_x(2 - 10 \text{ keV})^a$	$1.9 \times 10^{34}$	$1.9 \times 10^{34}$	$1.9 \times 10^{34}$	$2.6 \times 10^{34}$
$L_x(2 - 50 \text{ keV})^a$	$5.7 \times 10^{34}$	$5.7 \times 10^{34}$	$5.3 \times 10^{34}$	$6.7 \times 10^{34}$
$\chi^2_\nu$	0.869(69)	0.872(70)	1.02(70)	1.14(70)

NOTE—Quoted uncertainties are at the 90% confidence level for two interesting parameters.

<sup>a</sup>Unabsorbed luminosity, in erg s $^{-1}$ , for  $d = 9.8$  kpc (Blumer et al. 2019).

<sup>b</sup>Comptonized blackbody (CBB) parameter  $\alpha \equiv -\ln(\tau_{\text{es}})/\ln(A)$  tuned to match the modulation curve minimum. See Section 5.1 for details.

<sup>c</sup>Absorbed 2 – 10 keV flux, in erg cm $^{-2}$  s $^{-1}$ , from the *XMM-Newton* EPIC pn.

detail in Section 5.1 to further discriminate among the acceptable spectral models.

## 5. SPECTRAL ANALYSIS

Our previous analysis of J171405 showed that a variety of spectral models can fit the 0.3–10 keV *Chandra* and *XMM-Newton* data equally well, including two blackbodies, a blackbody plus power-law, and a Comptonized blackbody (Papers I, II). Now, the addition of the *NuSTAR* data, covering 3–79 keV, adds a strong spectral lever arm to help distinguish between these models. In the following sections, we use the spectral and energy-dependent modulation of the pulsar to show that its spectrum is best characterized by a Comptonized blackbody whose temperature is constant in time, plus an additional hard power-law. We also analyze the spectrum of the hard diffuse source XMMU J171410.8–381442, located 4.4' to the south of J171405, to consider its nature.

For spectral fitting we use the XSPEC (v12.8.2) package (Arnaud 1996) and characterize the column density with the built-in TBabs absorption model, selecting the wilm Solar abundances (Wilms et al. 2000) and the vern photoionization cross-section (Verner et al. 1996). The  $\chi^2$  statistic is used to evaluate the spectral fits throughout and the parameter uncertainties are quoted at the 90% confidence level for one or more interesting param-

eters, as appropriate. Response matrices and ancillary response files were generated for each data set following the standard procedures for their respective missions.

### 5.1. CXOU J171405.7–381031

In the current spectral study of J171405 we use all available *Chandra*, *XMM-Newton*, *NuSTAR* data sets<sup>1</sup>. Source spectra were extracted from circular apertures whose size were selected to optimize the signal to noise ratio for each observation. For the *Chandra* CC-mode data we extracted source spectra from the sum of the five central source columns, corresponding to a diameter of 2.''5 containing  $\approx 95\%$  of the point-source enclosed energy. The background in this case was obtained from the adjacent pixels on either side of the source region. We estimate the *NuSTAR* and *XMM-Newton* backgrounds using an annular region, to allow for underlying SNR emission in the source aperture. Because of the lack of available background regions for the *XMM-Newton* EPIC MOS data acquired in SmallWindowMode, only the EPIC pn data is used for spectroscopy. Spectra from the two *NuSTAR* FPMs were co-added.

<sup>1</sup> We excluded the 2007 *Chandra* observation in TE mode as it provides a poor flux measurement. The source was dithered on and off the edge of the CCD and suffers from time variable pile-up.

To characterize the broadband spectrum of J171405 we conducted a joint fit of the contemporaneous 2016 *XMM-Newton* and *NuSTAR* data. Several trial spectral models were fitted in the 1–10 keV and 3–65 keV range, for the two missions, respectively. With the addition of the harder *NuSTAR* spectra, we find that all single component models are rejected, including those allowed by previous fits to data below 10 keV, as reported in Paper II. Similarly, of the plausible two-component models, the two-blackbody model is also rejected due to a poor fit.

In contrast, we are able to obtain an excellent fit to the data (Figure 6) using an absorbed blackbody plus hard power-law model (BB+PL), with or without taking into account possible Compton scattering of the thermal emission (CBB+PL). For the latter, we use the model described in Halpern et al. (2008), where  $\alpha \equiv -\ln(\tau_{es})/\ln(A)$  is the log ratio of the scattering optical depth  $\tau_{es}$  over the mean amplification  $A$  of photon energy per scattering, valid for  $\tau_{es} \ll 1$  (Rybicki & Lightman 1986). The derived column densities for these models are consistent with the value reported for the SNR obtained using *Suzaku* data (Nakamura et al. 2009). While a fit using the double power-law model is formally acceptable, in this case the column density is far from that obtained for the SNR. A summary of spectral results for these models is presented in Table 2. Assuming a distance of 9.8 kpc (Blumer et al. 2019), the 2–50 keV X-ray luminosity of J171405 is  $\approx 5.7 \times 10^{34}$  erg s $^{-1}$ . This is comparable to its spin-down power,  $\dot{E} = 4\pi^2 I \dot{P}/P^3 \approx 5 \times 10^{34}$  erg s $^{-1}$  for  $P = 3.83$  s,  $\dot{P} = 7 \times 10^{-11}$ , and moment of inertia  $I = 10^{45}$  g cm $^2$ .

A further constraint on possible spectral models is provided by the energy-dependent modulation of the pulse profile as presented in Section 4. For the sum of two sinusoidally varying spectral components with the same period, but phase difference  $\Delta\phi$ , the net pulsed fraction  $f_p(E)$  as a function of photon energy  $E$  is predicted from their relative fluxes,  $F_1(E)$  and  $F_2(E)$ , as follows:

$$f_p(E) = \frac{f_1 F_1(E) \sin[\psi(E)] + f_2 F_2(E) \sin[\psi(E) + \Delta\phi]}{F_1(E) + F_2(E)},$$

where  $f_1$  and  $f_2$  are the (assumed energy-independent) pulsed fractions of the two spectral components, and

$$\psi(E) = \tan^{-1} \left[ \frac{f_1 F_1(E)}{f_2 F_2(E)} + \cos(\Delta\phi) \right] \sin(\Delta\phi)$$

is the energy-dependent phase shift. Of note, the modulation tends towards a minimum at the spectral cross-

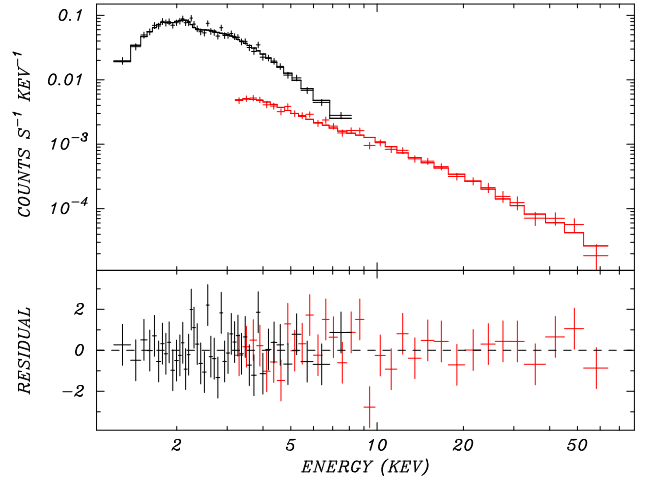


**Figure 6.** The broad-band X-ray spectrum of the magnetar J171405 in CTB 37B fitted to the absorbed Comptonized blackbody plus power-law model. Shown is the joint fit to the coincident 2016 *XMM-Newton* and *NuSTAR* data sets with model normalizations allowed to be independent. Upper panel: The data points (crosses) are plotted along with the best fit model (histogram) given in Table 2. Lower panel: The best fit residuals in units of sigma.

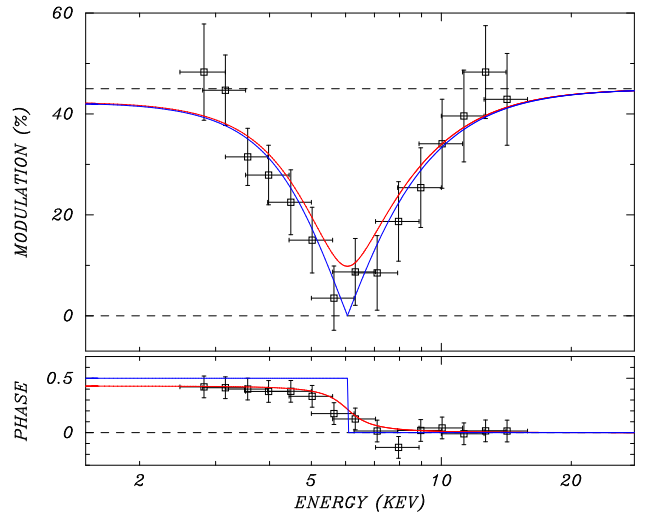


**Figure 7.** Energy-dependent modulation  $f_p(E)$  of J171405 computed using the 2016 *NuSTAR* observation. The modulation data points are derived from a sinusoidal fit to the background-subtracted pulse profiles, in overlapping logarithmically spaced energy bins. The energy dependence of the modulation and phase (solid lines) are modeled well by the ratio of the spectral components of the Comptonized blackbody plus power-law model (see Section 5.1), with  $f_1 = f_2 = 0.45$ . The model is computed for the observed pulse-phase offset of  $\Delta\phi = 0.43$  cycles between soft and hard X-rays (red line), and for a phase offset of  $\Delta\phi = 0.5$  cycles (blue line). Other spectral models are rejected because the cross-over energies of their components do not match the energy (6.1 keV) where the observed pulsed fraction is a minimum.



over energy, where the fluxes from the two spectral components are equal.

We apply this modulation model to the results of the joint fits to the coincident 2016 *XMM-Newton* and *NuSTAR* spectra for each spectral model of Table 2. Only the Comptonized blackbody plus power-law model is able to reproduce the observed modulation curve as a function of energy, specifically the location of the dip at 6.1 keV (Figure 7). The implied energy-independent modulation is 45% for both components, and the apparent phase offset is  $\Delta\phi = 0.43$  cycles. This offset between the phase of the blackbody and the power-law spectral components suggest that they arise on opposite sides of the neutron star, or possibly that the thermal emission is not viewed directly, but reflected by an opaque scattering screen (see Section 6).

The  $\chi^2_\nu$  of the CBB+PL spectral fit is smaller than that of the BB+PL model, justifying the extra parameter. But the modulation data provides a further constraint on the spectrum that allows us to distinguish between models, in this case implying deviations from pure blackbody emission. Furthermore, simultaneously fitting the spectra and modulation curve allows us to fine tune the spectral parameters for the CBB+PL model to adjust the spectral cross-over (6.6 keV) between components to match the dip in modulation at 6.1 keV. The tuned spectral parameters are well within the uncertainties of the nominal fit parameters for this model, resulting in a negligible change in the  $\chi^2_\nu$ , as presented in Table 2.

We now consider the full set of *Chandra*, *XMM-Newton*, and *NuSTAR* spectra acquired over a span of 8 years, from 2009 January 25 to 2017 February 22 (11 observations, see Table 1). Initial fits at each epoch shows no evidence of significant change in the spectral shape over time. We therefore fit all the spectra simultaneously with their normalization left free, to allow for calibration differences between telescopes and to search for flux variability. For ease of comparison, we use the nominal blackbody plus power-law model. The resulting combined fit is shown in Figure 8. The *NuSTAR* spectra, even if not generally taken at the same epoch as the other data sets, strongly constrain the temperature at the lower energies where the blackbody component dominates the *Chandra* and *XMM-Newton* spectra. The combined best fit model parameters are  $N_H = (3.88 \pm 0.16) \times 10^{22} \text{ cm}^{-2}$ , blackbody temperature  $kT = 0.60 \pm 0.015 \text{ keV}$ , and photon index  $\Gamma_2 = 0.95 \pm 0.19$ , with a  $\chi^2_\nu = 1.02$  for 601 degrees of freedom. This result is consistent with that presented in Table 2 for the coincident *XMM-Newton* and *NuSTAR* spectral fits.

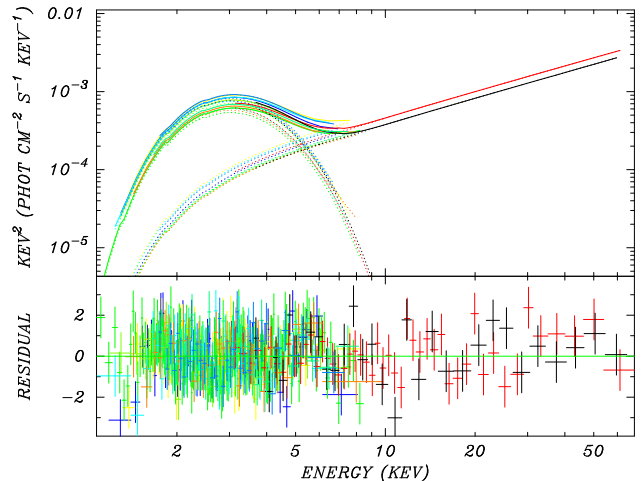


**Figure 8.** Broad-band X-ray spectra of the magnetar J171405 in CTB 37B at several epochs from year 2009 onwards, as listed in Table 1. Shown are *Chandra* ACIS, *XMM-Newton* EPIC pn, and *NuSTAR* FPM spectra fitted simultaneously to an absorbed blackbody plus power-law model. The model normalizations are independent between spectra. Upper panel: The data points (crosses) are plotted along with the best fit model (histogram). Lower panel: The best-fit residuals in units of sigma.

To study the long-term flux and spectral variability we refitted the individual spectra with column density and power-law index again linked between epochs, but with temperatures and normalizations free. The resulting temperature and flux for each observation are shown in Figure 9. We find no significant change in the time history of the temperature, but there is flux variability evidently uncorrelated with temperature. We quantify this variability by comparing a simultaneous fit across the 11 spectra with all parameters linked to one for which the blackbody normalization (only) is free to vary. The ratio of the resulting statistics,  $\chi^2 = 2.30(621)$  and  $\chi^2 = 1.04(610)$ , strongly excludes a constant flux model, with F-test probability  $\varphi < 1.5 \times 10^{-16}$ .

We note that this result does not take into account systematic differences in the inter-instrument flux calibrations or the photometric reproducibility of the individual instruments. However, we find that observations which are contemporaneous or adjacent have consistent fluxes, within their uncertainties. Interestingly, a possible exception is the highest flux point, in early 2010, which coincides with the brief doubling of  $\dot{P}$  in Figure 3. However, the data are otherwise too sparse to test for a relation between luminosity and spin-down rate.

The *XMM-Newton* and *Chandra* spectra used here were also analyzed by Watanabe et al. (2019), who found lower column densities, and 2–10 keV fluxes higher by  $\sim 30\%$  than ours. It is not clear what is responsible for these differences. Without the benefit of

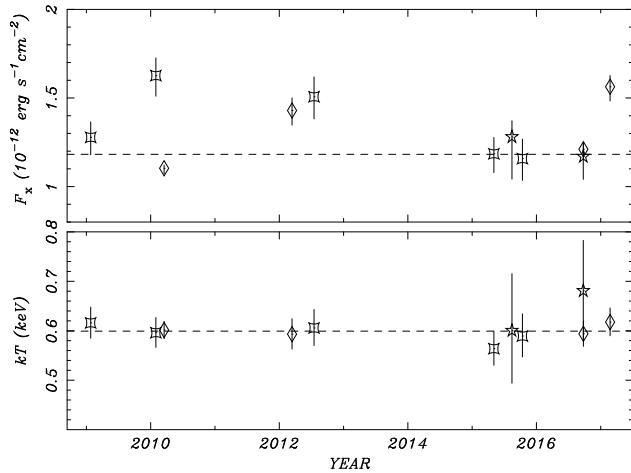


**Figure 9.** Time history of J171405 in CTB 37B. Plotted are the 2–10 keV fluxes (upper panel) and temperatures (lower panel) for *Chandra* (squares), *XMM-Newton* (diamonds), and *NuSTAR* (stars) spectra presented in Figure 8. The plotted errors are for the 90% confidence level.

the *NuSTAR* data, their spectral models do not account for the hard power-law component. They deemed the long-term flux variability to be insignificant.

### 5.2. XMMU J171410.8–381442

We extracted spectra from XMMU J171410.8–381442, the hard source to the south of CTB 37B, using data from the deep 2010 *XMM-Newton* and the 2016 *NuSTAR* observations. The source extraction aperture in the *XMM-Newton* data is shown in the lower right panel of Figure 2. The 2015 *NuSTAR* observation is not used, as the source region there is contaminated by stray light. For the *XMM-Newton* data, we restrict our analysis to the EPIC MOS data set due to the overwhelming background in the EPIC pn. The MOS spectrum is fitted in the 2–7 keV band, where the lower limit is chosen to avoid poorly subtracted, strong instrumental features. The *NuSTAR* spectrum is fitted in the 3–20 keV range, for lack of photons at higher energies. A total of 2310 MOS counts and 1010 FPM counts are extracted from the 2′ diameter aperture, of which 45% and 65% are background counts, respectively. The background regions for both spectra are chosen from a 4′ diameter aperture adjacent to the source region. With the lack of evidence for spectral features, we fit a simple absorbed power-law model. The best-fit parameters are  $N_H = (11 \pm 4) \times 10^{22} \text{ cm}^{-2}$ , and photon index  $\Gamma = 2.2^{+0.6}_{-0.5}$ , with a  $\chi^2_\nu = 0.62$  for 49 degrees of freedom. These results are somewhat different from the findings of Nakamura et al. (2009) from *Suzaku*, particularly our 2–10 keV unabsorbed flux of  $2.5 \times 10^{-13} \text{ erg cm}^{-2} \text{ s}^{-1}$ , which is half that reported by those authors. We consider the present results to be more reliable because

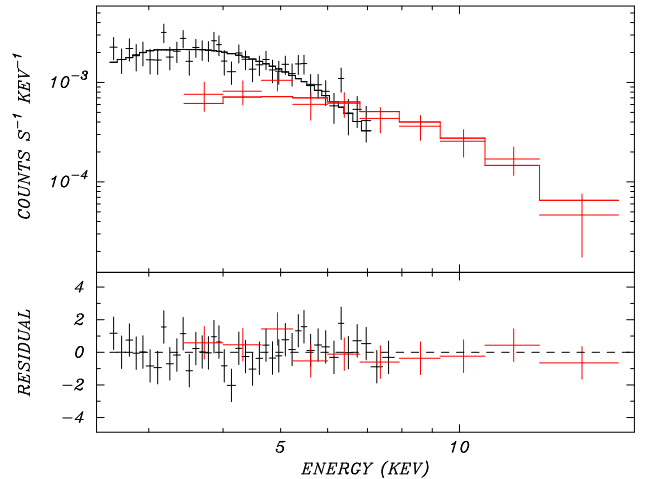


**Figure 10.** The broad-band X-ray spectrum of CXOU J171405.7–381031, the hard diffuse source south of CTB 37B, plotted along with the best fit absorbed power-law model (histogram) given in the text. The lower panel displays the residuals from the best fit model in units of sigma.

of the smaller PSF of *NuSTAR* and *XMM-Newton* in comparison to the *Suzaku* data, which suffered contamination from the nearby SNR and magnetar. The fitted column density to XMMU J171410.8–381442 is significantly higher than in the favored spectral model for J171405, which suggests that it might be unrelated to the magnetar or the SNR.

## 6. DISCUSSION AND CONCLUSIONS

The spectra of most magnetars are well-fitted below 10 keV with either a two-blackbody model or a blackbody plus a non-thermal power-law model with a steep  $\Gamma \approx 4$  slope. The latter model is similar to a Comptonized blackbody of appropriate scattering parameters. Evident non-thermal emission above 10 keV is characterized by a much flatter power-law with  $\Gamma \lesssim 1.5$ . The spectrum of J171405 is somewhat unusual in that the flux below 10 keV falls off much slower with energy than expected. In addition to a thermal component of  $kT \approx 0.6$ , notably, a hot thermal component ( $kT \approx 2.8 \text{ keV}$ ) or a flat ( $\Gamma \approx 0.8$ ) power-law component is required to fit the spectrum in this band. Because its power-law index is compatible with those from fits obtained above 10 keV, only two components are in fact required to fit the overall broad band spectrum of J171405.

For the magnetar spectral survey of Enoto et al. (2017), only four out of 15 objects that have a hard component above 10 keV can be satisfactorily fit with a single component in addition to their thermal spectra: SGR 1806–20, SGR 1900+14, 1E 1547.0–5408, and SGR 1833–0832. Furthermore, two more objects,

1E 1048.1–5937, and 1E 2259+586, show the need for either one or two components at different times, suggesting a correlation with their emission state. Like for SGR 1806–20 and SGR 1900+14, the hard power-law emission from J171405 might dominate and obscure a fainter thermal/power-law component. The spectral properties of J171405, shared by several of the SGRs, may therefore be attributes of its comparative youth and greater magnetic field strength relative to other AXPs, as shown in Figure 1. In fact, the spin-down rate, characteristic age, and surface magnetic field of J171405 are most similar to those of SGR 1900+14. And its hardness ratio, comparing the flux in the hard to soft bands, of  $F_{15-60 \text{ keV}}/F_{1-10 \text{ keV}} = 2.51$  agrees well with the correlations for those parameters reported by Enoto et al. (2017).

The energy-dependent modulation of J171405 is also unusual for a magnetar. In contrast with most magnetars, its pulsed fraction decreases with energy up to  $\approx 6$  keV, but this can be explained by the rising contribution of the hard spectral component, which happens to be phase-shifted by  $\approx 0.43$  cycles from the soft X-rays, thus reducing the net modulation. A similar effect is seen in 1RXS J170849.0–400910 (den Hartog et al. 2004), where a hard pulse component that dominates above 8 keV is shifted by  $\approx 0.4$  cycles from a soft pulse component below that energy.

The simplest interpretation of the phase shift would have the two spectral components arise from nearly opposite sides of the NS. However, in the Beloborodov (2013a,b) model of scattering from  $e^\pm$  pairs on twisted magnetic field-line bundles, the particles can form an opaque (to soft X-rays) resonance-scattering layer at the top of the magnetic loops, which obscures the surface hot spots from certain viewing angles. In this case, the thermal emission might not be seen directly, but could peak in reflection at the opposite phase.

For most other magnetars with hard pulsed components, the modulation increases with energy above 10 keV. Unfortunately the statistics of the *NuSTAR* data on J171405 are not sufficient above 30 keV to determine if its pulsed modulation continues to increase with photon energy above 10 keV, where the pulsed fraction reaches  $\approx 0.45$ . In some objects the pulsed fraction increases to as high as 0.96 at 20 keV (1E 2259+586: Vogel et al. 2014), while in others, the pulsed fraction levels off (4U 0142+61: Tendulkar et al. 2015; 1E1841–045: An et al. 2013, 2015) or decreases (1E1048.1–5937: Yang et al. 2016; XTE J1810–197: Gotthelf et al. 2019) at high energy.

Our original motivation for monitoring J171405 was to detect any timing and spectral changes that might

precede an SGR outburst, which could reveal the proximate cause of SGR flares. Based on the similarity of the timing properties of J171405 to the most energetic SGRs, an outburst can be expected, although we are still waiting for it. The factor of 2 change in  $\dot{P}$  that we observed is evidently not sufficient to trigger an outburst, even though it may be correlated with changes in X-ray luminosity. In other magnetars, an increase in torque has been seen *following* an outburst, by  $\sim 100$  days in 1E 1048.1–5937 (Archibald et al. 2015), and by  $\sim 1$  year in SGR 1820–20 (Woods et al. 2007; Younes et al. 2015), so it cannot be excluded that J171405 had an undetected bursting episode just prior to the beginning of our timing program.

The relation, if any, between the magnetar and HESS J1713–381 remains uncertain. There is no direct evidence from X-rays for a PWN that could contribute TeV emission. The existing *XMM-Newton* images are limited in their sensitivity to a PWN by the thermal X-ray emission from the SNR and the magnetar itself, while the deep imaging with *Chandra* that would be necessary to reveal a compact, nonthermal structure, has not yet been done. As discussed in Paper II, even though the *present* spin-down power of J171405 is only about equal to the TeV luminosity of HESS J1713–381, it is plausible that relic electrons, from a recent time when the  $\dot{E}$  was much larger than it is now, are powering a TeV nebula via inverse Compton scattering. GeV emission from *Fermi* has also been detected in the direction of CTB 37B (Xin et al. 2016), and its spectrum connects smoothly with that of HESS J1713–381, suggesting that there is only one  $\gamma$ -ray source at this location.

It is interesting that the only magnetar that has good evidence of possessing an X-ray PWN, Swift J1834.9–0846 (Younes et al. 2016), is also coincident with a SNR (W41), a TeV source (HESS J1834–097), and a GeV source (2FGL J1834.3–0848). Abramowski et al. (2015) discuss these associations in the context of the PWN possibly belonging to the nearby pulsar candidate XMMU J183435.3–084443 (Mukherjee et al. 2009), but it more likely belongs to Swift J1834.9–0846 (see also Misanovic et al. 2011). J171405 thus bears some similarity to Swift J1834.9–0846 in its associations.

The nearby source XMMU J171410.8–381442 is also a potential  $\gamma$ -ray emitter, although it is not clear whether it is part of the SNR shell of CTB 37B or an unrelated object. Its X-ray  $N_H$ , larger than that of the magnetar or the SNR, is tentative evidence that it may be a background source, e.g., a PWN. The GeV and TeV centroids are both closer to the magnetar and the SNR than to XMMU J171410.8–381442, although

there is room for overlap. This leaves the nature of XMMU J171410.8–381442 unknown. It could also be investigated with a deeper *Chandra* observation, e.g., to search for an embedded pulsar point source.

## ACKNOWLEDGMENTS

We thank the referee for making several informative suggestions. This investigation is based on new data obtained with the *NuSTAR* and *XMM-Newton* Observatories, and on archival data obtained with the *Chandra* Observatory. Support for this work was provided by NASA through *NuSTAR* Cycle 2 Guest Observer Program grant NNX17AC22G and through *XMM-Newton* Cycle 15 Guest Observer Program grant NNX17AC14G. The *NuSTAR* mission is a project led by the California Institute of Technology, managed by the Jet Propulsion Laboratory, and funded by the National Aeronautics and Space Administration. This research made use of the *NuSTAR* Data Analysis Software (NuSTAR-DAS) jointly developed by the ASI Science Data Center (ASDC, Italy) and the California Institute of Technology (USA). *XMM-Newton* is an ESA science mission with instruments and contributions directly funded by ESA member states and NASA. This research has made use of data and software provided by the *Chandra* X-ray Center (CXC) that is operated for NASA by the Smithsonian Astrophysical Observatory. Data and software were also provided by the High Energy Astrophysics Science Archive Research Center (HEASARC), which is a service of the Astrophysics Science Division at NASA/GSFC and the High Energy Astrophysics Division of the Smithsonian Astrophysical Observatory. We also acknowledge extensive use of the arXiv and the NASA Astrophysics Data Service (ADS). E.V.G. thanks Josep Maria Paredes for hosting his sabbatical at the University of Barcelona Institut de Ciències del Cosmos (ICCUB) and acknowledges support through the “Programa Estatal de Foment de la Investigació Científica i Tècnica d’Excellència, Convocatòria 2014, Unitats d’Excellència *Maria de Maeztu*.”

Facilities: *NuSTAR*, *CXO*, *XMM*

## REFERENCES

- Abramowski, A., Aharonian, F., Ait Benkhali, F., et al. 2015, *A&A*, 574, A27
- Aharonian, F., Akhperjanian, A. G., Bazer-Bachi, A. R., et al. 2006, *ApJ*, 636, 777
- Aharonian, F., Akhperjanian, A. G., Barres de Almeida, U., et al. 2008, *A&A*, 486, 829
- An, H., Hascoët, R., Kaspi, V. M., et al. 2013, *ApJ*, 779, 163
- An, H., Kaspi, V. M., Beloborodov, A. M., et al. 2014, *ApJ*, 790, 60
- An, H., Archibald, R. F., Hascoët, R., Kaspi, V. M., et al. 2015, *ApJ*, 807, 93
- Archibald, R. F., Kaspi, V. M., Ng, C.-Y., et al. 2015, 800, 33
- Arnaud, K. A. 1996, in *ASP Conf. Ser.* 101, *Astronomical Data Analysis Software and Systems V*, ed. G. H. Jacoby & J. Barnes (San Francisco, CA: ASP), 17
- Beloborodov, A. M. 2013a, *ApJ*, 762, 13
- Beloborodov, A. M. 2013b, *ApJ*, 777, 114
- Blumer, H., Safi-Harb, S. & Kothes, R. 2019, *MNRAS*, submitted (arXiv:1906.07249)
- Buccheri, R., Bennet, K., Bignami, G. F., et al. 1983, *A&A*, 128, 245

- Camilo, F., Scholz, P., Serylak, M., et al. 2018, *ApJ*, 856, 108
- den Hartog, P. R., Kuiper, L., Hermsen, W., & Vink, J. 2004, *ATel*, 293, 1
- den Hartog, P. R., Kuiper, L., & Hermsen, W. 2008, *A&A*, 489, 263
- Enoto, T., Shibata, S., Kitaguchi, T., et al. 2017, *ApJS*, 231, 847, L25
- Gotthelf, E. V., Halpern, J. P., Alford, J. A. J., et al. 2019, *ApJ*, 974, L25
- Green, A. J., Cram, L. E., Large, M. I., & Ye, T. 1999, *ApJS*, 122, 207
- Halpern, J. P., & Gotthelf, E. V. 2010a, *ApJ*, 710, 941 (Paper I)
- Halpern, J. P., & Gotthelf, E. V. 2010b, *ApJ*, 725, 1384 (Paper II)
- Halpern, J. P., Gotthelf, E. V., Reynolds, J., Ransom, S. M. & Camilo, F. 2008, *ApJ*, 676, 1178
- Harrison, F. A., Craig, W. W., Christensen, F. E., et al. 2013, *ApJ*, 770, 103
- Hascoët, R., Beloborodov, A. M., & den Hartog, P. R. 2015, *ApJ*, 786, L1
- Kaspi, V. M., Archibald, R. F., Bhalariao, V., et al. 2014, *ApJ*, 786, 84
- Madsen, K. K., Harrison, F. A., Markwardt, C. B., et al. 2015, *ApJS*, 220, 8
- Mereghetti, S., & Stella, L. 1995, *ApJ*, 442, L17
- Misanovic, Z., Kargaltsev, O., & Pavlov, G. G. 2011, *ApJ*, 735, 33
- Molkov, S. V., Cherepashchuk, A. M., Lutovinov, A. A., et al. 2004, *AstL*, 30, 534
- Mori, K., Gotthelf, E. V., Zhang, S., et al. 2013, *ApJ*, 770, L23
- Mori, K., Gotthelf, E. V., Dufour, F., et al. 2014, *ApJ*, 793, 88
- Mukherjee, R., Gotthelf, E. V., Halpern, J. P., et al. 2009, *ApJ*, 691, 1707
- Nakamura, R., Bamba, A., Ishida, et al. 2009, *PASJ*, 61, S197
- Revnivtsev, M. G., Sunyaev, R. A., Varshalovich, D. A., et al. 2004, *AstL*, 30, 382
- Rybicki, G. B., & Lightman, A. P. 1986, *Radiative Processes in Astrophysics*, (New York: Wiley-VCH)
- Sato, T., Bamba, A., Nakamura, R., & Ishida, M. 2010, *PASJ*, 62, L33
- Strüder, L., Briel, U., Dennerl, K., et al. 2001, *A&A*, 365, L18
- Tamba, T., Bamba, A., Odaka, H., & Enoto, T. 2019, *PASJ*, in press (arXiv:1906.04406)
- Tendulkar, S. P., Hascoët, R., Yang, C., et al. 2015, *ApJ*, 808, 32
- Turner, M. J. L., Abbey, A., Arnaud, M., et al. 2001, *A&A*, 365, L27
- van Paradijs, J., Taam, R. E., & van den Heuvel, E. P. J. 1995, *A&A*, 299, L41
- Verner, D. A., Ferland, G. J., Korista, K. T., & Yakovlev, D. G. 1996, *ApJ*, 465, 487
- Vogel, J. K., Hascoët, R., Kaspi, V. M., et al. 2014, *ApJ*, 789, 75
- Watanabe, H., Bamba, A., Shibata, S., & Watanabe, E. 2019, *PASJ*, in press (arXiv:1905.11561)
- White, R. L., Becker, R. H., & Helfand, D. J. 2005, *AJ*, 130, 586
- Wilms, J., Allen, A., & McCray, R. 2000, *ApJ*, 542, 914
- Woods, P. M., Kouveliotou, C., Finger, M. H. et al. 2007, *ApJ*, 654, 470
- Xin, Y.-L., Liang, Y.-F., Li, X., et al. 2016, *ApJ*, 817, 64
- Yang, C., Archibald, R. F., Vogel, J. K., et al. 2016, *ApJ*, 831, 80
- Younes, G., Kouveliotou, C., & Kaspi, V. M. 2015 *ApJ*, 809, 165
- Younes, G., Kouveliotou, C., Kargaltsev, O., et al. 2016 *ApJ*, 824, 138
- Younes, G., Baring, M. G., Kouveliotou, C., et al. 2017a *ApJ*, 851, 17
- Younes, G., Kouveliotou, C., Jaodand, A., et al. 2017b *ApJ*, 847, 85